

Measurement of fluid contents by light transmission in transient three-phase oil-water-air systems in sand

C. J. G. Darnault,^{1,2} D. A. DiCarlo,³ T. W. J. Bauters,¹ A. R. Jacobson,⁴
J. A. Throop,¹ C. D. Montemagno,¹ J.-Y. Parlange,¹ and T. S. Steenhuis¹

Abstract. Most three-phase flow models lack rigorous validation because very few methods exist that can measure transient fluid contents of the order of seconds of whole flow fields. The objective of this study was to develop a method by which fluid content can be measured rapidly in three-phase systems. The method uses the hue and intensity of light transmitted through a slab chamber to measure fluid contents. The water is colored blue with CuSO_4 . The light transmitted by high-frequency light bulbs is recorded with a color video camera in red, green, and blue and then converted to hue, saturation, and intensity. Calibration of hue and intensity with water, oil, and air is made using cells filled with different combinations of the three fluids. The results show that hue and water content are uniquely related over a large range of fluid contents. Total liquid content is a function of both hue and light intensity. The air content is obtained by subtracting the liquid content from the porosity. The method was tested with static and transient experiments. Measurements made with the light transmission method (LTM) and synchrotron X rays of the static experiment agreed well. In the transient experiments, fingers were formed by dripping water on the surface in a two-dimensional slab chamber with partially oil-saturated sand. The LTM is able to capture the spatial resolution of the fluid contents and can provide new insights in rapidly changing, three-phase flow systems.

1. Introduction

Groundwater pollution involving nonaqueous phase liquids (NAPLs) is threatening the environment and human health. NAPLs enter the vadose zone as a result of spills, inadequate disposal practices, or leaking underground storage facilities, thus contaminating groundwater resources [Schwille, 1988].

Effective remediation strategies require a good understanding of the transport processes of three-phase systems consisting of NAPLs, air, and water [Hunt *et al.*, 1988a, 1988b; Mercer and Cohen, 1990; Illangasekare *et al.*, 1995; Wilkins *et al.*, 1995]. Measuring the contaminant concentrations is an important factor in assessing risk to human health and the environment. Multiphase flow and transport phenomena in porous media are the focus of numerous research efforts [Abriola and Pinder, 1985a, 1985b; Pinder and Abriola, 1986; Abriola, 1989; Parker, 1989; Van Geel and Sykes, 1994; Blunt *et al.*, 1995; Miller *et al.*, 1997; Hashemi *et al.*, 1999]. Models incorporating multiphase flow and transport in the unsaturated and saturated zones of the subsurface environment have also been developed [Panday *et al.*, 1997; Muccino *et al.*, 1998]. Most of these multiphase models have not been rigorously validated for transient flow conditions because of the difficulty in measuring fluid contents. One of the less well understood transient flow phenomena in

three-phase systems is unstable fingering [Kueper and Frind, 1988; Held and Illangasekare, 1995; DiCarlo *et al.*, 1997]. Fingering decreases fluid retention time in the vadose zone, thus increasing groundwater contamination [Selker *et al.*, 1996]. Consequently, there is a need for fast, nondestructive, and accurate measurements of transient three-fluid phase flow in porous media.

Transient visualizations (but not direct measurement of fluid contents) have been made in Hele-Shaw cells with smooth walls [Saffman and Taylor, 1958; Chuoke *et al.*, 1959] or with imprints of porous media on glass [Schwille, 1988]. Currently, very few methods exist that allow rapid determination of fluid contents in three-phase, NAPL-air-water systems. Most of the available methods involve some form of radiation. These include dual-energy gamma radiation which measures multiphase fluid contents at a point [Ferrand *et al.*, 1986; Oostrom *et al.*, 1995], X-ray absorption (film-based radiography) described by Tidwell and Glass [1994], X-ray attenuation [McBride and Miller, 1994], and computerized tomography [Brown *et al.*, 1993; Morton *et al.*, 1999]. One method that does not use X rays is magnetic resonance imaging [Johns and Gladden, 1998]. The disadvantage of these methods is that they cannot measure transient flow phenomena. Synchrotron X rays allow for accurate and fast measurements of fluid contents in transient flow fields, in any soil type, but can measure only a small section of the flow field at one time because of the small beam size of 1 mm by 8 mm [DiCarlo *et al.*, 1997].

The objective of this research is to adapt the light transmission method (LTM) developed for two-phase flow systems [Darnault *et al.*, 1998] to three-phase flow systems. The advantages of the LTM are that it does not involve radiation and that it is able to visualize fluid content changes over the whole flow field with a time resolution of tenths of seconds. Spectroscopical analysis of the light transmitted through the calibration

¹Department of Agricultural and Biological Engineering, Cornell University, Ithaca, New York.

²Now at Malcolm Pirnie, Inc., Newport News, Virginia.

³Department of Petroleum Engineering, Stanford University, Stanford, California.

⁴Department of Crop and Soil Sciences, Cornell University, Ithaca, New York.































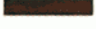

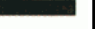





















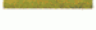


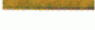


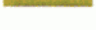


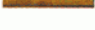

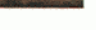
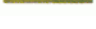

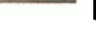
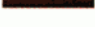


Water	Oil	Air	RGB	HUE	INTENSITY	Water	Oil	Air	RGB	HUE	INTENSITY
(cm ³ /cm ³)	(cm ³ /cm ³)	(cm ³ /cm ³)				(cm ³ /cm ³)	(cm ³ /cm ³)	(cm ³ /cm ³)			
0	0.380	0				0	0.380	0			
0	0.304	0.076				0.076	0.304	0			
0	0.228	0.152				0.152	0.228	0			
0	0.152	0.228				0.228	0.152	0			
0	0.076	0.304				0.304	0.076	0			
0	0	0.380				0.380	0	0			
0.076	0.076	0.228				0.380	0	0			
0.076	0.152	0.152				0.304	0	0.076			
0.076	0.228	0.076				0.228	0	0.152			
0.152	0.076	0.152				0.152	0	0.228			
0.152	0.152	0.076				0.076	0	0.304			
0.228	0.076	0.076				0	0	0.380			

Plate 1. Visualization of the different combinations of fluid contents (oil-water-air in 12/20 silica sand) from the calibration chamber under red, green, and blue (RGB), hue, and intensity image analysis.

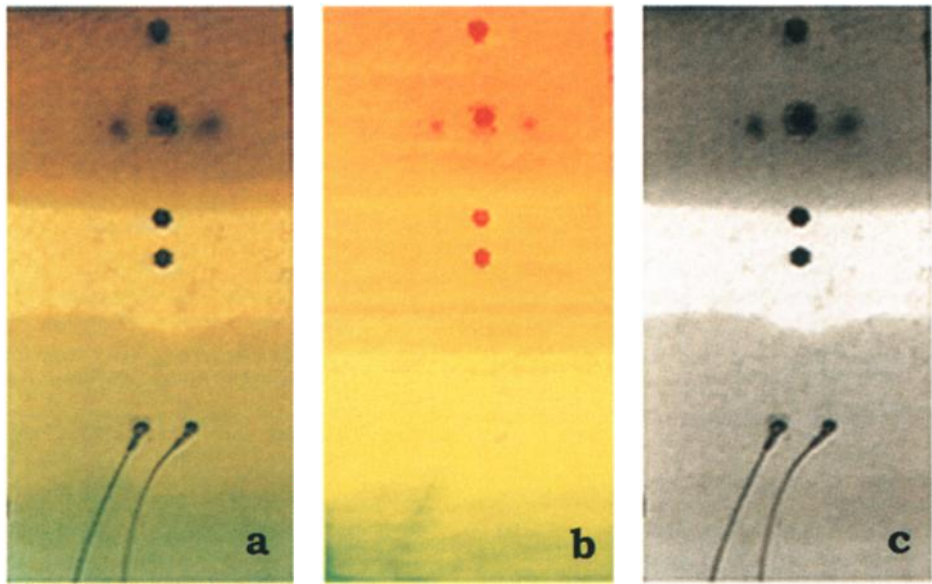


Plate 2. Visualization of a drainage experiment in soil-air-oil-water systems using (a) RGB system, (b) hue image, and (c) intensity image.

chamber and light source is performed. Fluid contents measured by the LTM are validated using synchrotron X rays (experiment 1). An unstable flow experiment in a soil-air-oil-water system demonstrates the versatility of the LTM (experiment 2).

2. Materials and Methods

2.1. Light Transmission Method

Color can be expressed in different formats; the most common are red, green, and blue (RGB) and hue, saturation, and intensity (HSI). In HSI format, hue is the color attribute that describes the pure color, saturation corresponds to the degree to which the color is diluted with white, and intensity corresponds to the gray level (black and white). The advantage of the HSI format is that it treats color roughly the same way that humans perceive and interpret color [Wilson, 1988]. Therefore, if the human eye is able to see differences in color and intensity for different fluid contents, these differences can be quantified using the HSI format. Previous experiments have shown that in air-water systems intensity is related to liquid content [Hoa, 1981; Glass *et al.*, 1989]. In oil-water systems in which the water is colored blue, hue is related to water content [Darnault *et al.*, 1998]. We can expect therefore that in three-phase systems consisting of air, water, and oil, hue and intensity can describe the water content and total liquid content, respectively.

For fluid measurements in porous media the LTM involved placing a two-dimensional chamber in front of a uniform light source and recording the transmitted light [Darnault *et al.*, 1998]. Experiments were performed at a constant temperature of 20°C. A light source composed of a bank of 24 fluorescent, high-frequency light bulbs located in front of a white background was used. The transmitted light was recorded with a Sony color video camera employing three 0.5 inch (1.25 cm) charge couple devices (CCD) images, each having a total of 250,000 effective picture elements. The camera was located 1 m in front of the chamber with constant settings (zoom of 0.95 m and aperture of f5.6). The images were stored on a Hi8 video cassette in RGB format. In order to convert RGB to HSI, hue (H) can be expressed as [Wilson, 1988]

$$H = 225 \left\{ \frac{1}{360} \left[Y - \arctan \frac{2R - G - B}{\sqrt{3}(G - B)} \right] \right\} \quad (1)$$

$$Y = 90 \quad G > B, \quad Y = 270, \quad G < B,$$

where R , G , and B are the red, green, and blue intensities, respectively. The value for Y depends on the green and blue intensities. Intensity (I) is calculated as [Wilson, 1988]

$$I = 255 \left(\frac{R + G + B}{3} \right). \quad (2)$$

Values of H and I range from 0 to 255.

Recorded images were converted from RGB to HSI format and analyzed using a Power Macintosh equipped with a video digitizer (RasterOps 24 XLT from RoasterOps Corporation, 1992) and scientific image processing software (IPLab Spectrum V3.00 software from Signal Analytics Corporation, 1989–1995).

2.2. Calibration

To obtain a calibration curve between hue and water content and between intensity and total liquid (water and oil) content,

a two-dimensional calibration chamber consisting of cells filled with a porous media and known quantities and fluid ratios of oil-water, air-water, oil-air, or air-oil-water was constructed. The oil used was Soltrol 220, a transparent isoparaffine solvent composed of a mixture of alkanes C13 through C17 from the Phillips 66 Company. The distilled water was dyed blue with CuSO_4 at a concentration of 28% which was found to give the widest range of hue values for the different moisture contents. The calibration chamber was 62 cm high, 52 cm wide, and 1 cm thick. It was divided into 24 cells 3 cm high by 23 cm wide. The cell walls were constructed from the same 1 cm thick Hyzod polycarbonate sheet (Sheffield Plastic, Inc.) as the experimental chamber. Walls between the cells were painted black to avoid edge effects from the transmitted light. The cells were packed to a porosity of 38% with 20/30 sieve size, industrial quartz silica sand (Union Corporation) with particle sizes between 0.66 and 0.83 mm. The sand-packed cells were then filled with all possible fluid combinations. The fluid contents of each of the three fluids were varied by $0.076 \text{ cm}^3/\text{cm}^3$ increments (Plate 1).

To obtain an accurate calibration, it was important to have uniform sand packing as well as homogeneously mixed fluids. To achieve this, we found by experience that various methods were needed to fill the cells with the different fluid mixtures. To obtain the required liquid contents for cells that simultaneously contained all three liquids (i.e., air, water, and oil) predetermined quantities of oil, water, and sand were added to a beaker, then stirred, and packed into the cell by vibration. For cells filled with only two liquids (air-water, air-oil, or water-oil) several filling procedures were required to achieve a uniform fluid distribution. Cells that contained 0.076 and $0.152 \text{ cm}^3/\text{cm}^3$ of either water or oil with air as the second fluid were mixed and packed with the same procedure as used for the three liquids. For the cells that contained 0.228 , 0.304 , and $0.380 \text{ cm}^3/\text{cm}^3$ of either oil or water, again with air as the second fluid, the predetermined quantities of liquid were added first to the cells followed by the dry sand. Capillary action spread the liquid uniformly across the cell. To obtain the liquid contents in the oil- and water-saturated sands an injection method was used. In the oil-water system, at the 0.076 and $0.152 \text{ cm}^3/\text{cm}^3$ water contents, the required quantity of water was mixed with the sand in a beaker, stirred, and packed by vibration into the cell and followed by an injection of the oil from the bottom of the cell through a hypodermic tube previously installed along the corner of the cell walls. For the 0.228 and $0.304 \text{ cm}^3/\text{cm}^3$ water contents 0.057 and $0.076 \text{ cm}^3/\text{cm}^3$, respectively, of the required quantity of water and the total quantity of oil were added to sand in a beaker. The mixture was mixed and packed by vibration in the cell, and then the remaining quantity of water was injected with a syringe at the bottom of each cell through the (previously installed) hypodermic tube.

For each cell the hue and intensity were measured as the mean values in a centered rectangle, 100 pixels long (16 cm) by 5 pixels (0.8 cm) wide. These average values were plotted versus the corresponding water and liquid contents to obtain the calibration curves.

2.3. Spectroscopy

To gain a better understanding of the LTM, the light spectrum emitted from the light source and the transmitted light from each cell of the calibration chamber were measured using a PC 1000S spectrometer from Ocean Optics, Inc., and Spec-

taScope version 2.1 software. Light was captured by placing the end of a 0.4 mm diameter by 2 m long fiber optic against the walls of the cells of the calibration chamber or the glass in front of the light source. Six points, measured every 3 cm across each cell, were analyzed. The brightest cell was used to adjust the signal gain, before measuring the spectrum, to avoid saturation.

2.4. Synchrotron X rays

X-ray measurements of the fluid contents in the soil-air-oil-water systems were performed at the F-2 beam line at the Cornell High-Energy Synchrotron Source (CHESS), using dual-energy attenuation measurements. These consist of an initial white X-ray beam which is reflected off a double-bounce Si(220) monochromator producing a beam of two distinct energies (20 and 40 Kev) that enter the experimental hutch. This technique was developed by DiCarlo *et al.* [1997].

2.5. Experiments

Static and transient flow experiments were performed with a slab chamber. The experimental chamber had 1 cm thick polycarbonate walls and interior dimensions of 45 cm width, 1 cm thickness, and 55 cm height. To give more rigidity to the experimental chamber and to prevent expansion, the sides of the chamber were constructed of solid, 6 cm wide polycarbonate. A manifold of five fluid ports was located at the bottom (Figure 1). The chamber was filled with either water or oil to a predetermined level to achieve the initial experimental conditions. Silica (20/30) sand was added continuously through a funnel-extension-randomizer assembly. The experimental chamber was continuously vibrated. A 10 cm sand layer was maintained in the funnel to achieve natural packing with uniform density and to avoid movement of the sand particles during the experiment. After packing, the top 2 cm of sand were removed by sweeping, bringing the sand height to 55 cm. It was observed that the liquid attenuated the vibrations so that the placement of a soil-air system above a soil-oil or soil-air-oil system resulted in a lower packing density in the soil-air system. Differences in density affect the amount of light transmitted. As discussed in section 3.1, these effects can be eliminated by recording the amount of light transmitted by the chamber before the water is added.

Two experiments were performed to test the validity and versatility of the LTM. In experiment 1 the accuracy of the LTM in determining water, oil, and air contents was compared with synchrotron X rays for an oil-water-air system. For this experiment the slab was filled with 20/30 quartz silica sand. Oil (Soltrol 220) was then injected slowly from the bottom to 45 cm of the slab height followed by drainage down to 15 cm. Then, water was injected slowly from the bottom up to 30 cm. Finally, the slab was drained to 25 cm. After the drainage was stopped, the synchrotron X-ray measurements were taken followed by the LTM measurements. Three layers and two transition zones could be distinguished. Starting at the bottom, there was a 5 cm layer of water-saturated sand, a 5 cm transition zone to a 20 cm layer of primarily oil-saturated sand, and a 15 cm transition zone to a 5 cm layer of air-saturated sand. Some air and water entrapment was observed within the different layers and transition zones.

Experiment 2 was a transient flow experiment consisting of unstable fingered flow in a porous media of quartz silica sand. The experimental chamber was filled with 15 cm of oil. Then, 20/30 sand was added, resulting in oil-saturated sand to 42 cm

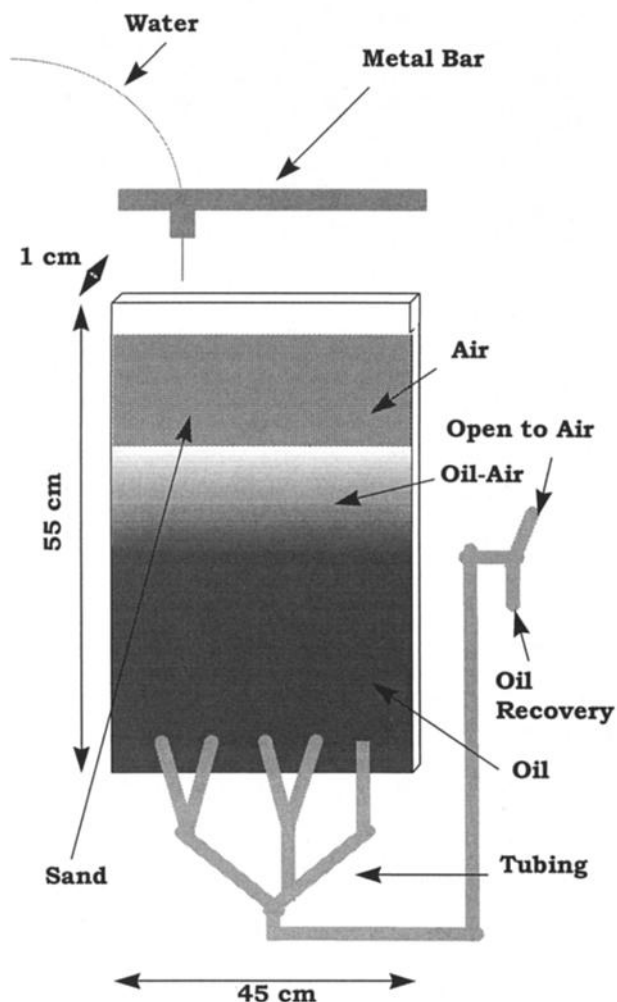


Figure 1. Experimental setup.

and air-saturated sand from 42 to 55 cm. The experimental chamber was then drained, resulting in three different zones with (from bottom to top): 10 cm oil-saturated sand (0–10 cm), a mixture of oil and air (10–32 cm) with a capillary fringe of 10 cm (32–42 cm), and dry sand (42–55 cm). To form a finger, water was applied as a point source through a needle 1 cm above the sand surface at a rate of 3 mL/min. The oil level was kept constant via overflow tubing located 1 cm below the oil in the chamber placed at 31 cm. A series of seven vertical profiles was analyzed for fluid content at the center of the finger as the finger progressed into the different sand-oil-air saturated phases and interfaces. Also, four cross-horizontal scans of 7, 19.5, 27.2, and 37 cm depths of the fluid content of the fully formed finger corresponding to the different sand-oil-air phases were measured. Cross sections were labeled A, B, C, and D, respectively, and are depicted in Plate 3 that is presented later.

3. Results and Discussion

3.1. Calibration

The relationship for water, oil, and air contents as a function of hue, intensity, and porosity was developed using the calibration chamber. Differences in hue and intensity between the different cells of the calibration chamber could be observed by

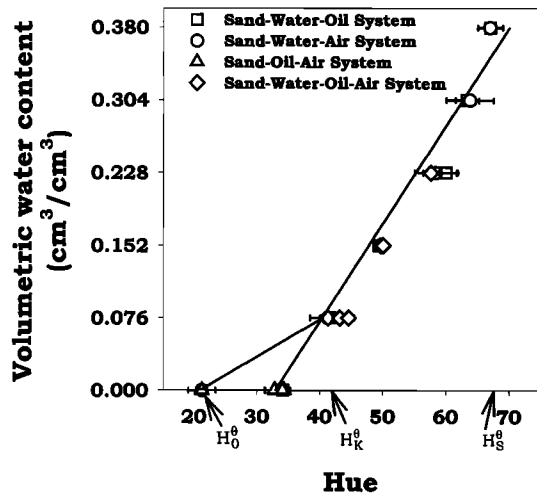


Figure 2. Water contents in soil-oil-water-air systems versus hue values.

eye (Plate 1). The air-saturated cell was brown and dark; the oil-saturated cell was yellow and bright; the water-saturated cell was blue-green and dark; and finally, the oil-water-saturated and air-oil-water-saturated cells appeared bright in various shades of green. The hue and intensity were obtained by converting the images from RGB to HSI format with the IPLab Spectrum software from Signal Analytics Corporation (1989–1995). The hue values were represented according to the 1976 chromaticity diagram of the Commission Internationale de l'Eclairage, and the intensity values were displayed in gray scale. The hue values ranged from brown, the lowest hue value (20), to blue, the highest hue value (70), while the intensity values ranged from black, the lowest intensity value (20), to white, the highest value (220).

Different equations were used to relate H (hue) to θ_w (water content) above and below $0.076 \text{ cm}^3/\text{cm}^3$ (Figure 2). Above a water content of $0.076 \text{ cm}^3/\text{cm}^3$ the hue and water content were uniquely related, independent of oil and air contents; while below a water content of $0.076 \text{ cm}^3/\text{cm}^3$, the hue value depends on the oil and air contents in the chamber.

At water contents above $0.076 \text{ cm}^3/\text{cm}^3$ the water content could be obtained by

$$\theta_w = 0.076 + 0.304 \left(\frac{H - H_K^0}{H_S^0 - H_K^0} \right) \quad 0.076 < \theta_w \leq \theta_s, \quad (3)$$

where θ_w is the volumetric water content, H is the hue of the transmitted light, H_K^0 is the hue at $0.076 \text{ cm}^3/\text{cm}^3$ water, and H_S^0 is the hue at $0.38 \text{ cm}^3/\text{cm}^3$ water (saturation).

Below water contents of $0.076 \text{ cm}^3/\text{cm}^3$ the relationship between water content and hue was dependent on the oil content in the soil and can be approximated as

$$\theta_w = 0.076 \left(\frac{H - H_0^0}{H_K^0 - H_0^0} \right) \quad 0 \leq \theta_w \leq 0.076, \quad (4)$$

where θ_w is the volumetric water content, H is the hue of the transmitted light, H_0^0 is the initial hue at $0 \text{ cm}^3/\text{cm}^3$ water, and H_K^0 is the hue at $0.076 \text{ cm}^3/\text{cm}^3$ water from the calibration chamber.

This dependence of the hue value on both oil and water contents for water below $0.076 \text{ cm}^3/\text{cm}^3$ requires an iterative process to find the oil and water contents. In some instances,

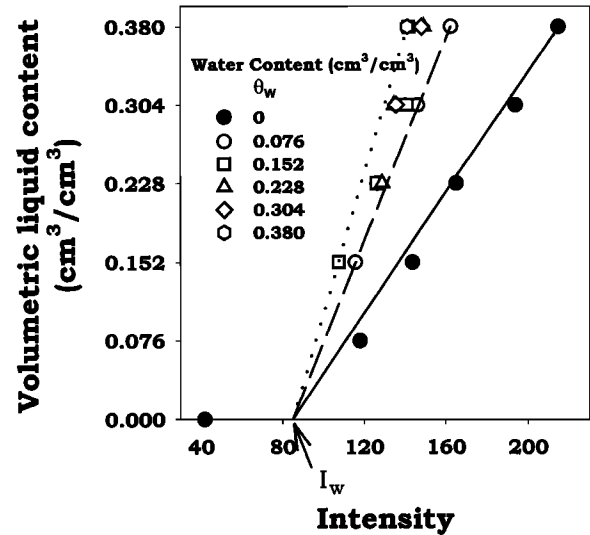


Figure 3. Liquid content in soil-oil-air-water systems versus intensity values.

additional information can be used to calculate the water content without the iterative process by using information from scans before the experiment was started. The details are given in section 3.4 when the results of the experiments are described.

Previously, it was found that for soils with only water without dye the intensity was linearly related to total liquid content [Bauters *et al.*, 2000]. Since the blue dye in the water absorbed some of the light, the intensity for our experiments was not uniquely related to total liquid content but, rather, depended on both the oil and water contents (Figure 3). For liquid contents $>0.076 \text{ cm}^3/\text{cm}^3$, we found that for each water content there is a linear relationship between total liquid content and intensity (Figure 3). The lines converged at an anchor point, I_w , with a slope that was a function of the corresponding water content. A simple relationship between liquid content and intensity could be developed by substitution of the intensity value at the anchor point (85) for the observed intensity value at $0 \text{ cm}^3/\text{cm}^3$ liquid content (40). The substitution did not introduce significant error into the relationship because initial experimentation showed that at $0.02 \text{ cm}^3/\text{cm}^3$ liquid content the intensity was close to 85. Liquid contents below $0.02 \text{ cm}^3/\text{cm}^3$ can be found directly assuming a linear relationship between intensity and fluid content. A scan before each experiment allowed us to analyze the intensity values at the initial conditions. Packing density differences produced small variations in the intensity of the transmitted light, though not the hue, in the sand-air system. Thus intensity values emanating from a sand-air system were first corrected by the factor ζ . The factor can be found as the ratio of the intensities in the experimental chamber and the cell at any liquid content. In practice, however, the factor ζ is found as the ratio of the initial intensity value observed for air-dried sand in the experimental chamber to the intensity value measured for air-dried sand in the calibration.

Thus, for constant water content, the liquid content, θ_L , can be found as

$$\theta_L = \theta_s \left[\frac{(\zeta I - I_w)}{I_s(\theta_w)} \right] \quad 0.076 < \theta_L \leq \theta_s, \quad (5)$$

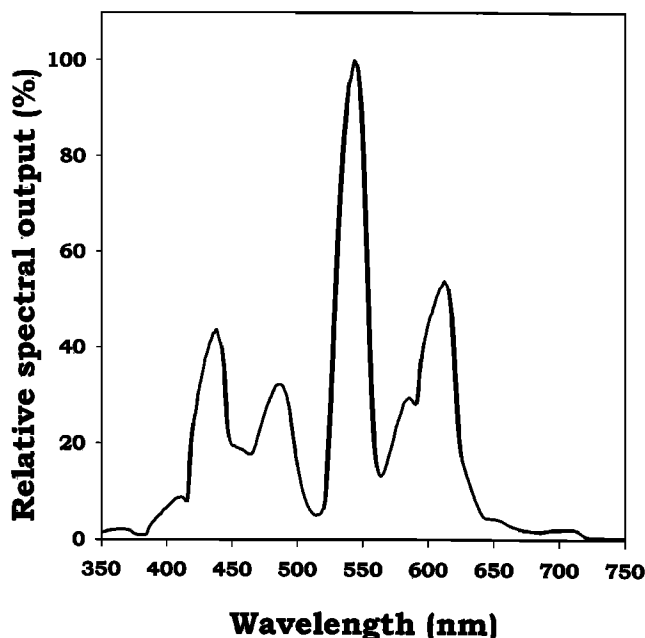


Figure 4. Relative spectral output of the light source.

where θ_s is the saturated volumetric liquid content, equal to $0.38 \text{ cm}^3/\text{cm}^3$, I is the observed intensity, ζ is the correction factor, I_w is the intensity value of the anchor point, and $I_s(\theta_w)$ is the saturated liquid intensity value with a water content, θ_w .

To find the saturated liquid intensity value, $I_s(\theta_w)$, two sets of equations are used depending if the water content is above or below $0.076 \text{ cm}^3/\text{cm}^3$:

$$I_s(\theta_w) = (I_0^\theta - I_w) - \frac{\theta_w}{0.076} (I_0^\theta - I_K^\theta) \quad 0 \leq \theta_w \leq 0.076, \quad (6)$$

$$I_s(\theta_w) = (I_K^\theta - I_w) - \frac{(\theta_w - 0.076)}{0.304} (I_K^\theta - I_s^\theta) \quad 0.076 < \theta_w \leq \theta_s, \quad (7)$$

where θ_w is the volumetric water content calculated by (3) and (4), I_0^θ is the intensity for $0.38 \text{ cm}^3/\text{cm}^3$ oil, I_K^θ is the intensity for $0.076 \text{ cm}^3/\text{cm}^3$ water with $0.304 \text{ cm}^3/\text{cm}^3$ oil, I_s^θ is the intensity for $0.38 \text{ cm}^3/\text{cm}^3$ water, and I_w is the intensity of the anchor point. For liquid contents below $0.03 \text{ cm}^3/\text{cm}^3$ we used a linear relationship between the observed intensity and the intensity of air-dried sand with an intensity value (40).

The oil and air contents, θ_o and θ_A , were obtained from the liquid content and porosity:

$$\theta_o = \theta_L - \theta_w, \quad (8)$$

$$\theta_A = \theta_s - \theta_L. \quad (9)$$

In summary, for hue values above 40 the water content is determined first with (3), followed by the determination of liquid content using (7). The oil and air contents are obtained with (8) and (9). Below hue values of 40 an iterative process is needed to find the oil and water contents in the soil.

3.2. Spectroscopy

The spectrophotometer measurements of the light source (Figure 4), and the cells of the calibration chamber (Figures 5

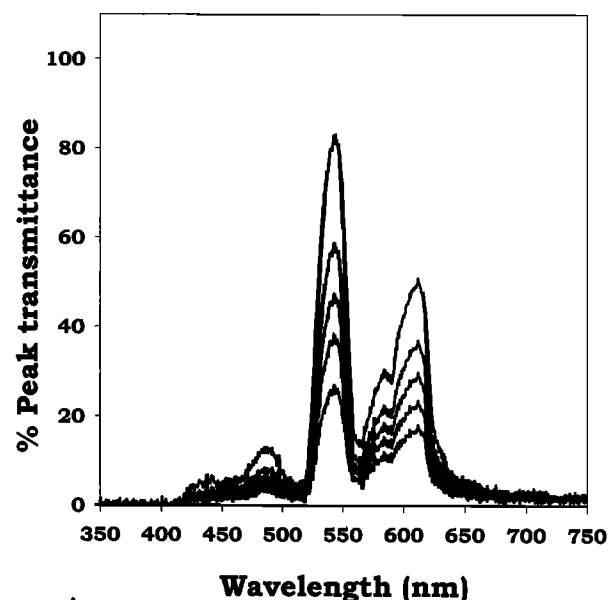


Figure 5. Transmittance spectrum of cells filled with soils that have the same water content and different oil content. The lines from top to bottom are for cells with soils that contain $0.076 \text{ cm}^3/\text{cm}^3$ of water and $0.304, 0.228, 0.152, 0.076, 0 \text{ cm}^3/\text{cm}^3$ of oil, respectively.

and 6), provide insight into the remarkable relationship between hue and intensity and their corresponding liquid contents. The relative spectral output of the light source, calculated with reference to its highest peak at 544 nm , displays four main peaks: 438 nm (purple), 485 nm (blue), 544 nm (green), and 612 nm (red) (Figure 4). Examples of the percentage peak transmittance spectra for calibration cells containing 0.076

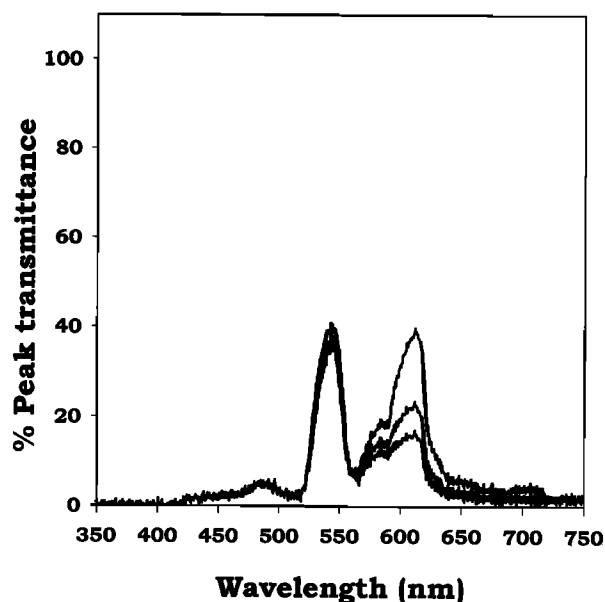


Figure 6. Transmittance spectrum of cells filled with 0 soils that have a liquid content of $0.152 \text{ cm}^3/\text{cm}^3$. The top line is for the cell with $0.152 \text{ cm}^3/\text{cm}^3$ of oil and no water; the line in the middle is for the soil with $0.076 \text{ cm}^3/\text{cm}^3$ water and $0.076 \text{ cm}^3/\text{cm}^3$ oil; the bottom line is for the cell that contains $0.152 \text{ cm}^3/\text{cm}^3$ of water and no oil.

cm^3/cm^3 water, and all the other possible combinations of fluids, and $0.152 \text{ cm}^3/\text{cm}^3$ liquid, and all the other possible combinations of water and oil, are presented (Figures 5 and 6). As with the light source spectral output, the percentage peak transmittance spectra of the calibration cells is calculated with reference to the wavelength yielding the highest peak transmittance: 544 nm for the oil-saturated system. The percentage peak transmittance spectra for the calibration cells shows the same main peaks but each at distinct transmission levels (Figures 5 and 6). The sand absorbs relatively more light at wavelengths above 510 nm than at lower wavelengths. As expected from the calibration chamber results in Plate 1, the transmittance pattern for the different cells is unique. For cells with a water content of $0.076 \text{ cm}^3/\text{cm}^3$ (Figure 5), transmittance increases with increasing oil contents, but the ratio of transmittance at the green (544 nm) and red (612 nm) peak wavelengths remains approximately constant. This confirms the results in Plate 1 that, while intensity increases with increasing liquid contents, the hue remains the same. In the cells with $0.152 \text{ cm}^3/\text{cm}^3$ of liquid (Figure 6) the transmittance of the peak at 612 nm decreases with increasing water content, while the transmittance at the 544 nm peak is minimally affected by the water content. In other words, the red transmittance decreases as the water becomes bluer, while the green transmittance is only minimally affected, thus resulting in the differences in hue apparent in Plate 1.

3.3. Experiment 1: Validation

A color image (as seen by the video camera in RGB format) of experiment 1 setup is shown in Plate 2a. The various oil, air, and water contents are clearly distinguishable. From the bottom up, several colors are visible: blue (water), blue green (water and oil), yellow (oil), dark yellow (oil and air), and brown (air). The red, green, and blue intensities for each pixel of the image were then converted with (1) and (2) to hue and intensity values. The hue and intensity values are shown in Plates 2b and 2c using the same convention as in Plate 1. Visualization of hue (Plate 2b) and intensity (Plate 2c) allows the qualitative and quantitative characterization of water content and liquid content, respectively, as well as their spatial distribution. From the bottom up in Plate 2b the hues range from green to yellowish red: green (water-saturated porous media), yellow (water-oil-air-saturated porous media), reddish yellow (oil-saturated porous media), and yellowish red (oil-air-saturated porous media). Similarly, in Plate 2c from the bottom up the intensity ranges from bright to dark, indicating liquid-saturated (oil and water) to air-saturated porous media, respectively. The hue and intensity values from (1) and (2) were then used to calculate the water and liquid contents. The hue value at zero water, H_0^0 (4), was taken at 32 to account for the background hue of the experimental setup. The oil content was obtained by subtracting the water content from the liquid content.

In Figure 7 both water and oil contents are depicted with depth and compared with those obtained with the synchrotron X rays. In general, the fluid contents with depth compare well though the oil content is lower at ~ 35 cm depth and higher at ~ 17 cm depth. These differences might have been caused by transporting the chamber some 500 m from the soil and water laboratory to the synchrotron. Since neither measurement technique gives the true value, we can only compare statistically how well both methods agree. A regression analysis with zero intercept between the fluid content measurements by the

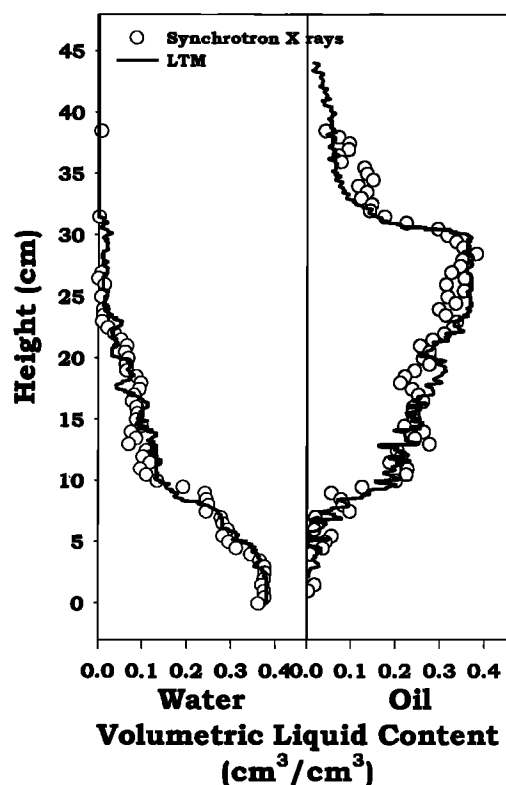


Figure 7. Vertical fluid contents profile from the drainage experiment using the light transmission method and synchrotron X rays.

synchrotron X rays (independent variable) and the LTM (dependent variable) indicates a regression coefficient (R^2) of 0.97 for water and 0.92 for oil. The slopes are 1.03 for both fluids with a standard error between the two measurement techniques of $0.023 \text{ cm}^3/\text{cm}^3$ for water and $0.037 \text{ cm}^3/\text{cm}^3$ for oil. The slightly larger standard error for the oil is expected since the LTM uses the water content to calculate the oil content.

3.4. Experiment 2: Transient Flow

Plate 3 shows a water finger emanating from a point source at different times as it moves first into the dry sand (fingers 1 and 2), then into partially oil-saturated sand (fingers 3, 4, and 5) and, finally, into oil-saturated sand (fingers 6 and 7). Plate 3a shows the image recorded by the video camera. Plates 3b and 3c depict the corresponding hue and intensity values. Prior to each transient flow experiment, a scan of the fluid-saturated (oil and air) sand in the experimental chamber was made to determine the initial H_0^0 used in (4). Fluid content profiles for the fully formed finger 7 are depicted in Figures 8 and 9. As expected from previous experiments [Glass *et al.*, 1989; Selker *et al.*, 1992; Liu *et al.*, 1994; Rimmer *et al.*, 1998; DiCarlo *et al.*, 1999] and as clearly observed in Plate 3b (fingers 1 to 7), the tip of the finger is the wettest (i.e., light green), while the remainder of the finger is much dryer (yellowish tint). Near the surface the finger is again wetter, which is typical when water is dripped on a surface [Bauters *et al.*, 2000]. Fingertip fluid contents for the time series in Plate 3 are shown in Table 1. Surprisingly, the oil content for the finger tips is highest in the partially saturated oil medium.

Plate 3a shows that in all zones the finger does not expand

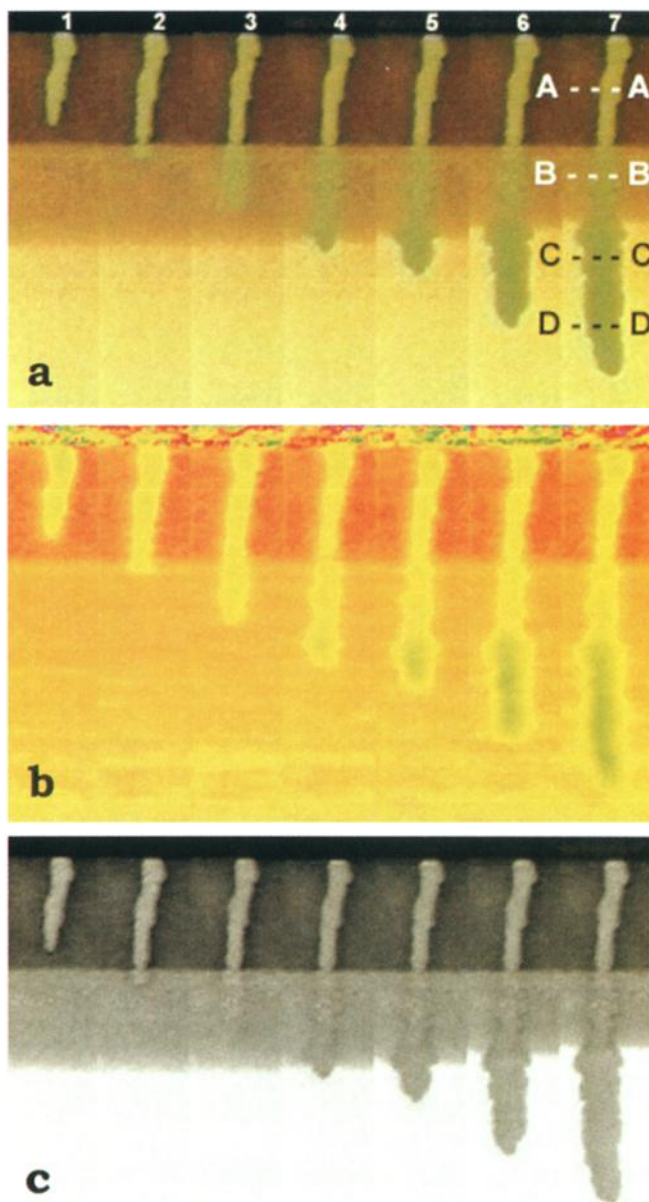


Plate 3. Seven time series visualization of water fingering phenomena in soil-air-oil system using (a) RGB system, (b) hue image, and (c) intensity image.

once it is formed. This is characteristic of unstable finger formation and is caused by hysteresis in the soil constitutive relationships [Glass *et al.*, 1989]. The finger core is on the drainage branch, while the surrounding fluid is on the imbibing branch, making it possible to have a high water content (drainage branch) and low water content (imbibing branch) at the same matrix potential. Thus both two- and three-phase systems exhibit typical, unstable flow behavior. This is distinctly different from the dissolution fingers observed in experiments by Imhoff and Miller [1996] and Imhoff *et al.* [1996]. In their experiments, water was pumped through a two-phase system containing trichloroethylene (TCE) and water. Unlike our experiments, fingers grew as a function of the distance traveled, eventually spanning the whole chamber.

In order to compare the results of the present experiment with previous findings in two-phase systems, we measured the

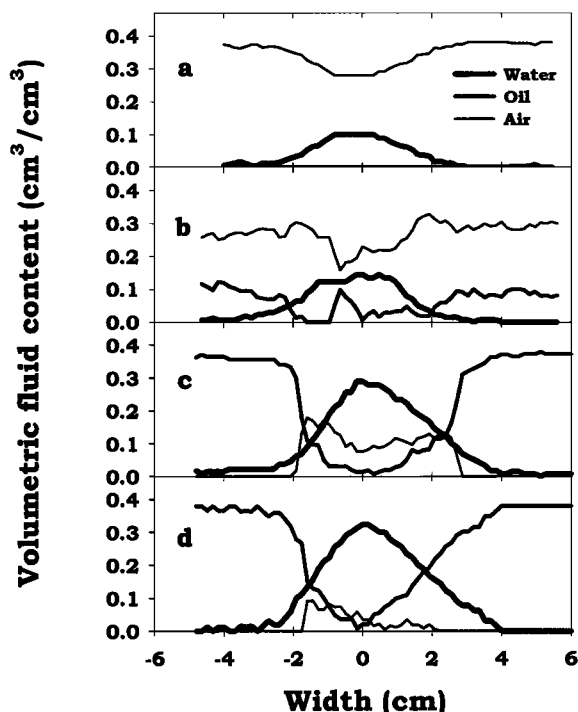


Figure 8. Four horizontal fluid content scans of the water finger (7) in the soil-air-oil system at depths of (a) 7 cm, (b) 19.5 cm, (c) 27.2 cm, and (d) 37 cm.

finger widths by calculating the difference between points corresponding to half the maximum water content using Figure 8. These measurements show that the finger width increases from 2.5 cm in the initially air-dried sand near the surface to 3.5 cm

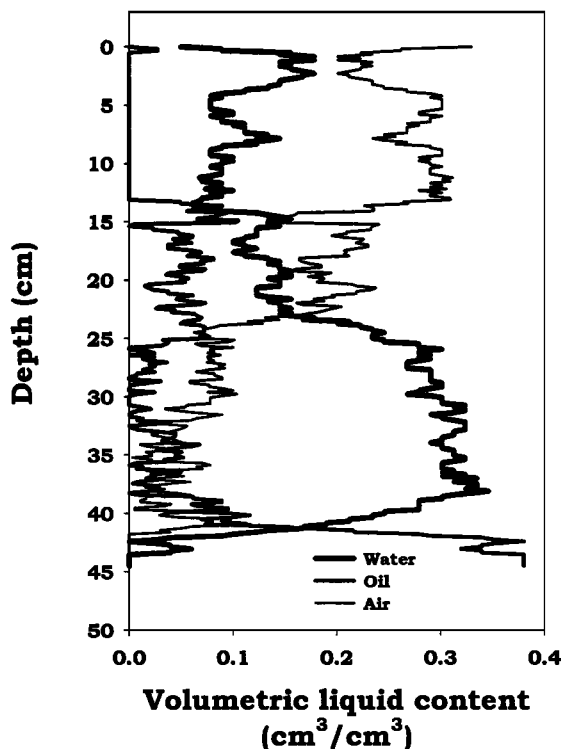


Figure 9. Vertical fluid content profile of a water finger in soil-air-oil system (7).

Table 1. Fluid Contents for Fingertips in Experiment 2^a

Finger	Water Content, cm ³ /cm ³	Oil Content, cm ³ /cm ³	Air Content, cm ³ /cm ³	Depth, cm
1	0.16	0.00	0.22	7.5
2	0.16	0.00	0.22	12.5
3	0.16	0.10	0.12	17
4	0.18	0.06	0.14	24
5	0.28	0.0	0.10	26
6	0.32	0.01	0.05	32
7	0.35	0.02	0.01	38

^aThe finger numbers refer to time series in Plate 3.

in the sand containing oil ganglia. Near the bottom of the oil-saturated sand the finger width is 5 cm (Figure 8). Finger widths in the air-dried sand and oil-saturated sand were in agreement with earlier findings (Table 2) using the same 20/30 sand [Liu et al., 1994; DiCarlo et al., 1997; Chandler et al., 1998; Rimmer et al., 1998]. Finger diameter for oil-saturated sand is twice that for air-dried sand and is in accordance with earlier studies [Chandler, 1998]. The finger width in the initially partially oil-saturated soil falls between the experimentally determined widths of the two-phase systems (air-water and oil-water). Several studies have reported that NAPL ganglia trapped in the porous media greatly reduce the permeability of the medium to aqueous phase flow [Imhoff and Miller, 1996; DiCarlo et al., 1997]. Since finger width is a direct function of the ratio of sorptivity squared to hydraulic conductivity [Chandler et al., 1998; Rimmer et al., 1998] and only increases slightly from air-dried to partially oil-saturated sand, this means that sorptivity and conductivity due to the presence of ganglia decrease at approximately the same rate. This can be specified in more detail by determining the constitutive relationship by using the LTM measurements in conjunction with simultaneous matrix potential measurements with the method described by DiCarlo et al. [1999].

Of final interest, is the liquid content of the finger when it reaches the bottom of the chamber. Its vertical and horizontal fluid content profiles have been calculated based on its hue and intensity values ((3), (4), (8), and (9)). The vertical fluid content profiles are presented in Figure 9. Horizontal cross sections of the fluid content at 7, 19.5, 27.2, and 37 cm, for a finger that has reached the bottom of the chamber, are shown in Figure 8. Although the unstable flow theory for unstable finger formation is not yet developed for three phases, our results show that unstable finger behavior in three-phase systems exhibits many similarities to that in two-phase systems.

Table 2. Finger Widths in 20/30 Sand Resulting From Water Infiltration in Air-Dried Sand Without Oil (Air), Partially Saturated With Oil (Air/Oil), and Saturated With Oil (Oil)

Experiment	Finger Diameter, cm		
	Air	Air/Oil	Oil
This study	2.5	3.5	5
Chandler et al. [1998]			4.8 (±1) ^a
Rimmer et al. [1998]			4.6
DiCarlo et al. [1997]	2.3 (±0.3) ^a		
Liu et al. [1994]	2.25		

^aThe number in parentheses is the standard deviation when known.

4. Conclusion

The light transmission method (LTM) is a nondestructive method that allows measurement of fluid contents in transient air-oil-water flow occurring in sandy, porous media. The LTM is an effective tool for investigating three-phase flow systems: air, oil, and water. The LTM has been found to yield reliable fluid contents in steady state, air-oil-water flow fields, as verified by comparing the results of a static experiment with synchrotron X rays. In transient measurements the LTM is capable of representing the fast changing fluid contents with high temporal resolution. The advantage of the LTM is that it records the fluid contents of the entire flow in less than 0.1 s (the time it takes for a video camera to take an image), so that we are able to analyze, qualitatively and quantitatively, fingering phenomena in soil-air-oil-water systems. Qualitative data, such as observations of the phenomena, and quantitative data, such as the dimensions, velocity, and fluid contents of the flow, are of primary importance in understanding flow patterns in soil-air-oil-water systems. Additionally, the LTM is able to provide data to validate one-dimensional and two-dimensional computer codes for transient air, oil, and water flow, to develop models of three-phase flow phenomena, to simulate groundwater pollution scenarios, and to simulate effective groundwater remediations, such as those using surfactants. The main disadvantage of LTM, relative to a method such as the synchrotron X ray, is that the measurements depend on the translucence of the porous medium and therefore require the use of silica sand. The unique ability of the LTM to map the complete flow phenomenon in less than 0.1 s more than compensates for this limitation. The other limitation of both LTM and X-ray measurement techniques is that relatively thin two-dimensional slabs are required for obtaining fluid contents. Since this drawback cannot easily be solved, three-dimensional transient fluid observations will still have to wait a while.

Acknowledgment. This work was sponsored by the U.S. Air Force Office of Scientific Research under grant/contract number F49620-94-1-0291.

References

- Abriola, L. M., Modeling multiphase migration of organic chemicals in groundwater systems: A review and assessment, *Environ. Health Perspect.*, 83, 117–143, 1989.
- Abriola, L. M., and G. F. Pinder, A multiphase approach to the modeling of porous media contaminated by organic compounds, 1, Equation development, *Water Resour. Res.*, 21, 11–18, 1985a.
- Abriola, L. M., and G. F. Pinder, A multiphase approach to the modeling of porous media contaminated by organic compounds, 2, Model development, *Water Resour. Res.*, 21, 19–26, 1985b.
- Bauters, T. W. J., D. A. DiCarlo, T. S. Steenhuis, and J.-Y. Parlange, Soil water content dependent wetting front characteristics in sands, *J. Hydrol.*, 231–232, 244–254, 2000.
- Blunt, M., D. Zhou, and D. Fenwick, Three-phase flow and gravity drainage in porous media, *Transf. Porous Media*, 20, 77–103, 1995.
- Brown, G. O., M. V. Stone, and J. E. Gazin, Accuracy of gamma ray computerized tomography in porous media, *Water Resour. Res.*, 29, 479–486, 1993.
- Chandler, D. G., Z. Cohen, E. Wong, D. A. DiCarlo, T. S. Steenhuis, and J.-Y. Parlange, Unstable fingered flow of water into a light oil, in *Hydrology Days*, edited by H. Morel-Seytoux, pp. 13–31, AGU, Washington, D. C., 1998.
- Chuoque, R. L., P. van Meurs, and C. van der Poel, The instability of slow, immiscible viscous, liquid-liquid displacement in porous media, *Trans. Am. Inst. Min. Metall. Pet. Eng.*, 216, 188–194, 1959.
- Darnault, C. J. G., J. A. Throop, A. Rimmer, D. A. DiCarlo, T. S. Steenhuis, and J.-Y. Parlange, Visualization by light transmission of

- oil and water contents in transient two-phase flow fields, *J. Contam. Hydrol.*, **31**, 337–348, 1998.
- DiCarlo, D. A., T. W. J. Bauters, T. S. Steenhuis, J.-Y. Parlange, and B. R. Bierck, High-speed measurements of three-phase flow using synchrotron x rays, *Water Resour. Res.*, **33**, 569–576, 1997.
- DiCarlo, D. A., T. W. J. Bauters, C. J. G. Darnault, T. S. Steenhuis, and J.-Y. Parlange, Rapid determination of constitutive relations with fingered flow, in *Proceedings of International Workshop on Characterization and Measurements of the Hydraulic Properties of Unsaturated Porous Media*, edited by M. T. van Genuchten, F. J. Leij, and L. Wu, pp. 433–440, Univ. of Calif., Riverside, 1999.
- Ferrand, L. A., P. C. D. Milly, and G. F. Pinder, Dual-gamma attenuation for the determination of porous medium saturation with respect to three fluids, *Water Resour. Res.*, **22**, 1657–1663, 1986.
- Glass, R. J., T. S. Steenhuis, and J.-Y. Parlange, Mechanism for finger persistence in homogeneous, unsaturated, porous media: Theory and verification, *Soil Sci.*, **148**, 60–70, 1989.
- Hashemi, M., B. Dabir, and M. Sahimi, Dynamics of two-phase flow in porous media: Simultaneous invasion of two fluids, *AIChE J.*, **45**, 1365–1382, 1999.
- Held, R. J., and T. H. Illangasekare, Fingering of dense nonaqueous phase liquids in porous media, 1, Experimental investigation, *Water Resour. Res.*, **31**, 1213–1222, 1995.
- Hoa, N. T., A new method allowing the measurements of rapid variations of the water content in sandy porous media, *Water Resour. Res.*, **17**, 41–48, 1981.
- Hunt, J. R., N. Sittar, and K. S. Udell, Non-aqueous phase liquid transport cleanup, 1, Analysis of mechanisms, *Water Resour. Res.*, **24**, 1247–1258, 1988a.
- Hunt, J. R., N. Sittar, and K. S. Udell, Non-aqueous phase liquid transport cleanup, 2, Experimental studies, *Water Resour. Res.*, **24**, 1259–1269, 1988b.
- Illangasekare, T. H., J. L. Ramsey Jr., K. H. Jensen, and M. B. Butts, Experimental study of movement and distribution of dense organic contaminants in heterogeneous aquifers, *J. Contam. Hydrol.*, **20**, 1–25, 1995.
- Imhoff, P. T., and C. T. Miller, Dissolution fingering during the solubilization of nonaqueous phase liquids in saturated porous media, 1, Model predictions, *Water Resour. Res.*, **32**, 1919–1928, 1996.
- Imhoff, P. T., G. P. Thyrum, and C. T. Miller, Dissolution fingering during the solubilization of nonaqueous phase liquids in saturated porous media, 2, Experimental observations, *Water Resour. Res.*, **32**, 1929–1942, 1996.
- Johns, M. L., and L. F. Gladden, MRI study of non-aqueous phase liquid extraction from porous media, *Magn. Reson. Imaging*, **16**, 655–657, 1998.
- Kueper, B. H., and E. O. Frind, An overview of immiscible fingering in porous media, *J. Contam. Hydrol.*, **2**, 95–110, 1988.
- Liu, Y., T. S. Steenhuis, and J.-Y. Parlange, Formation and persistence of fingered flow fields in coarse grained soils under different moisture contents, *J. Hydrol.*, **159**, 187–195, 1994.
- McBride, J. F., and C. T. Miller, Nondestructive measurements of phase fractions in multiphase porous-media experiments by using x-ray attenuation, *Cent. Multiphase Res. News*, **1**, 10–13, 1994.
- Mercer, J. W., and R. M. Cohen, A review of immiscible fluids in the subsurface: Properties, models characterization and remediation, *J. Contam. Hydrol.*, **6**, 107–163, 1990.
- Miller, C. T., G. Christakos, P. T. Imhoff, J. F. McBride, J. A. Pedit, and J. A. Trangenstein, Multiphase flow and transport modeling in heterogeneous porous media: Challenges and approaches, *Adv. Water Resour.*, **21**, 77–120, 1997.
- Morton, E. J., R. D. Luggar, M. J. Key, A. Kundu, L. M. N. Tavora, and W. B. Gilboy, Development of a high speed x-ray tomography system for multiphase flow imaging, *IEEE Trans. Nucl. Sci.*, **46**, 380–384, 1999.
- Muccino, J. C., W. G. Gray, and L. A. Ferrand, Toward an improved understanding of multiphase flow in porous media, *Rev. Geophys.*, **36**, 401–422, 1998.
- Oostrom, M., J. H. Dane, B. C. Missildine, and R. J. Lenhard, Error analysis of dual-energy gamma radiation measurements, *Soil Sci.*, **160**, 28–42, 1995.
- Panday, S., Y. S. Wu, P. S. Huyakorn, S. C. Wade, and Z. A. Saleem, A composite numerical model for assessing subsurface transport of oily wastes and chemical constituents, *J. Contam. Hydrol.*, **25**, 39–62, 1997.
- Parker, J. C., Multiphase flow transport in porous media, *Rev. Geophys.*, **27**, 311–328, 1989.
- Pinder, G. F., and L. M. Abriola, On the simulation of nonaqueous phase organic compounds in the subsurface, *Water Resour. Res.*, **22**, 109S–119S, 1986.
- Rimmer, A., D. A. DiCarlo, T. S. Steenhuis, B. Bierck, D. Durnford, and J.-Y. Parlange, Rapid fluid content measurement method for fingered flow in an oil-water-sand system using synchrotron x-rays, *J. Contam. Hydrol.*, **31**, 315–335, 1998.
- Saffman, P. G., and G. Taylor, The penetration of a fluid into a porous medium or Hele Shaw cell containing a more viscous liquid, *Proc. R. Soc. London Ser. A*, **245**, 312–331, 1958.
- Schwille, F., *Dense Chlorinated Solvents in Porous and Fractured Media*, translated from German by J. F. Pankow, Lewis, Chelsea, Mich., 146 pp., 1988.
- Selker, J. S., T. S. Steenhuis, and J.-Y. Parlange, Fingered flow in two dimensions, 2, Predicting finger moisture profile, *Water Resour. Res.*, **28**, 2525–2528, 1992.
- Selker, J. S., T. S. Steenhuis, and J.-Y. Parlange, An engineering approach to fingered vadose pollutant transport, *Geoderma*, **70**, 197–206, 1996.
- Tidwell, V. C., and R. J. Glass, X-ray and visible light transmission for laboratory measurement of two-dimensional saturation fields in thin-slab systems, *Water Resour. Res.*, **30**, 2873–2882, 1994.
- Van Geel, P. J., and J. F. Sykes, Laboratory and model simulations of a LNAPL spill in a variably-saturated sand, 2, Comparison of laboratory and model results, *J. Contam. Hydrol.*, **17**, 27–53, 1994.
- Wilkins, M. D., L. M. Abriola, and K. D. Pennel, An experimental investigation of rate limited nonaqueous phase liquid volatilization in unsaturated porous media: Steady state mass transfer, *Water Resour. Res.*, **31**, 2159–2172, 1995.
- Wilson, A., What is color? *Electron. Syst. Design Mag.*, **38**, 4, 1988.
- T. W. J. Bauters, C. J. G. Darnault, C. D. Montemagno, J.-Y. Parlange, T. S. Steenhuis, and J. A. Throop, Department of Agricultural and Biological Engineering, Riley-Robb Hall, Cornell University, Ithaca, NY 14853. (tbauters@yahoo.com; CDarnault@pirnie.com; cdm11@cornell.edu; jp58@cornell.edu; tssl@cornell.edu; jat12@cornell.edu)
- D. A. DiCarlo, Department of Petroleum Engineering, Stanford University, Stanford, CA 94305. (dicarlo@pangea.stanford.edu)
- A. R. Jacobson, Department of Crop and Soil Sciences, Bradfield Hall, Cornell University, Ithaca, NY 14853. (arj5@cornell.edu)

(Received May 10, 2000; revised November 2, 2000; accepted November 15, 2000.)